Magnetophonon resonance in double quantum wells

D. Ploch, E. M. Sheregii, M. Marchewka, M. Wozny, and G. Tomaka
Institute of Physics, University of Rzeszów, Rejtana 16a, Rzeszów 35-959, Poland
(Received 27 October 2008; revised manuscript received 6 April 2009; published 27 May 2009)

The experimental results obtained for the magnetotransport in pulsed magnetic fields in the InGaAs/InAlAs double quantum well (DQW) structures of two different shapes of wells and different values of the electron density are reported. The magnetophonon resonance (MPR) was observed for both types of structures within the temperature range 77–125 K. Four kinds of LO phonons are taken into account to interpret the MPR oscillations in the DQW and a method of the Landau level calculation in the DQW is elaborated for this aim. The peculiarity of the MPR in the DQW is the large number of the Landau levels caused by SAS splitting of the electron states (splitting on the symmetric and anti-symmetric states) and the large number of the phonon assistance electron transitions between Landau levels. The significant role of the carrier statistics is shown too. The behavior of the electron states in the DQWs at comparably high temperatures has been studied using the MPR. It is shown that the Huang and Manasreh [Manasreh [Phys. Rev. B **54**, 2044 (1996)] model involving screening of exchange interaction is confirmed.

DOI: 10.1103/PhysRevB.79.195434 PACS number(s): 73.21.Fg, 73.63.Hs, 72.15.Gd

I. INTRODUCTION

The experimental studies of the electron transport in the double quantum well (QW) (DQW) structures have been reported in several publications in the last two decades. These experiments have demonstrated new and interesting phenomena which were not observed in the structures with the single two-dimensional-gas (2DEG) layer. One is the absence of some integer quantum Hall states caused by splitting of the electron states into symmetric and antisymmetric states (so called SAS gap or Δ_{SAS} in DQW systems[1,2]).

In the structures where the barrier is thin enough, the SAS gap plays a decisive role. The magnitude of this splitting can be directly determined by means of current-voltage characteristics of such structures; it was also proved that the SAS gap is proportional to the applied magnetic field.[3] This dependence was attributed by Huang and Manasreh[4] to the screening of the exchange interaction in the DQW structures by electrons, which leads to the collapse of Δ_{SAS} in the absence of magnetic fields.

Among new phenomena, the Bose condensation,[5] Wigner crystallization,[6,7] and the long-time nuclear-lattice relaxation in DQW (Refs. 8 and 9) were observed in the structures with strongly correlated 2DEG in DQW at very low temperatures. Therefore, if we consider the electrons in the strongly correlated DQW structures, there is a possibility to treat them as two separate subsystems: one belonging to symmetric states, the other to antisymmetric states. The symmetric and antisymmetric states differ from each other because the symmetric properties of their wave functions are different. It leads to different quasi-Fermi levels for these states at low temperatures.[10] Therefore, the symmetric and antisymmetric states in DQWs are characterized by different statistics at low temperatures similar to two states with opposite spins. It is interesting whether this property is retained at higher temperatures.

The method of the Landau level (LL) energies calculation including the screening of the exchange interaction should be elaborated for DQW. According to the theory presented in Ref. 4, the Δ_{SAS} appears again and increases in a strong magnetic field because the screening is removed by the magnetic field. It is important to verify this theoretical prediction experimentally in a wide range of magnetic fields and temperatures. In particular, the magnetophonon resonance (MPR) (Ref. 11) in pulsed magnetic fields of the order of 35 T enables us to examine this conception in the temperature range from 77 to 300 K. It is appropriate because of the forecasted applications of DQWs (both double quantum wells and double quantum wires) are related to the quantum computation and quantum circuits working in the same temperature interval.[12] Simultaneously, the peculiarity of the electron-phonon interaction and the transport properties of the 2DEG in the DQWs should be studied.

In this work the data on MPR obtained in strong-pulsed magnetic fields (up to 37 T) for the InGaAs/InAlAs DQW are presented and analyzed. The analysis is based on the correct calculation of the Landau level energies in QWs as well as on the conception of deformed tetrahedral basic cells of the phonon spectra in the ternary solid solutions[13] which form the QWs and barriers in the DQWs.

II. THEORY

The MPR oscillations connect two subsystems of crystal or low-dimensional structure—electrons and phonons; hence the theoretical aspect of the MPR in the DQWs should concern two subjects: the electron subsystem in external magnetic field (Landau quantization in DQWs) and interaction of conductive electrons with the phonon subsystem in the DQWs.

A. Electron-phonon interaction in DQW

In the case of DQWs, electrons are moving in the multimode medium of two channels: two of the QWs limited (separated) by barriers. They (QWs and barriers) are often built with ternary alloys. The crystalline structure of these ternary solid solutions (mainly the fcc) is characterized by

tetrahedra, each with a central ion surrounded by four nearest neighbors (NNs) in the first coordination shell at the vertices. In the $A_xB_{1-x}Z$ ternary tetrahedron structures, different tetrahedron configurations T_n (n is the number of B atoms in the tetrahedron) coexist simultaneously: two strictly binary ones corresponding to the AZ and the BZ compounds whose lattices are characterized by the tetrahedron units T_0 and T_4 (configurations), respectively, and three strictly ternary ones actually characterized by the configurations T_1, T_2, and T_3. In an ideal crystal lattice, they all generate together at least $(2\times1)+(3\times2)=2+6=8$ optically active phonon modes. These are canonical phonon modes (CPMs) (Ref. 14) expressed by the formula for an imaginary part of the dielectric function,

$$\text{Im}\ \epsilon(\omega)=\sum_{i=1}^{k}\frac{S_i\gamma_i\omega}{(\omega_{\text{TO}i}^2-\omega^2)^2+\omega^2\gamma_i^2}, \tag{1}$$

where S_i, $\omega_{\text{TO}i}$, and γ_i are the oscillator strength, frequency, and damping parameter of the i-phonon mode, respectively.

Except for the bulk phonons, the surface or interface can generate a phonon mode also. Therefore, the phonon subsystem in the DQWs is characterized by a considerable number of phonon modes. This peculiarity of the phonon subsystem should be reproduced in the electron transport as a diversification of the electron-phonon interaction and can appear in the MPR as additional series of peaks similarly to the bulk crystals of the CdHgTe,[15,16] ZnCdHgTe,[17] and MnCdHgTe (Ref. 18) alloys. In case of MPR in the heterostructures and superlattices, except the additional series,[19–24] the subtle structure of peaks was also observed.[25] It means that each phonon mode produces its own polar potential[26]

$$V_q^s=\frac{\hbar\omega_{\text{LO}s}}{qu^{1/2}}\left(\frac{4\pi\alpha_s}{V}\right)^{1/2} \tag{2}$$

where $u=(2m^*\omega_{\text{LO}s}/\hbar)^{1/2}$, α_s, and LO_s are the Frölich constant and phonon frequency for sth phonon mode, respectively, and V is the volume of crystal, m^* is the electron effective mass.

Electron interacting with these separated potentials can absorb the phonon energy corresponding to the oscillation frequency in the multimode lattice, according to the resonance condition,

$$E'-E=\hbar\omega_{\text{LO}s}, \tag{3}$$

where E' and E are the LL energies of the final and initial electron states, respectively.

The phonon modes in barriers produce polar macropotential, which can penetrate in the QW as was shown earlier[19] by micro-Raman experiment. Therefore, electron movement in the channels of the DQW can interact with different kinds of LO phonons producing the separate polar potential [Eq. (2)]. They are created by the lattice in both of these channels (QW) and by the barriers surrounding these channels as well as caused by the interfaces.

B. LLs energies in DQWs

The Landau quantization theory of the in-plane motion electron in a DQW should take into account a screening in the form of the Hartree-Fock self-consistent potential.[4] In this model the screened exchange interaction is calculated using a generalized Thomas-Fermi screening method and the self-consisted Hartree potentials $V_H(z)$ should be involved in the Schrödinger equation containing the DQW potential $V_{\text{DQW}}(z)$. So, in an external magnetic field applied perpendicularly to the planes of quantum wells, using Hartree-Fock approximation, the electron motion in the z direction perpendicular to the DQW is described by[4]

$$\left[-\frac{\hbar^2}{2}\frac{d}{dz}\left(\frac{1}{m^*(z)}\frac{d}{dz}\right)+V_{\text{DQW}}(z)+V_H(z)\right]\phi_j(z)=E_j\phi_j(z), \tag{4}$$

where $j=1,2,\ldots$ is the subband index and m^* is the position-dependent effective mass of electrons. Meanwhile, the in-plane electron motion in each subband in the DQW is Landau quantized according to the equation,

$$\left[-\frac{\hbar^2}{2m_j^*}\frac{d^2}{dx^2}+\frac{1}{2}m_j^*\omega_{cj}^2(x-X_0)^2\right]\xi_{nk_y}(x)=\left(n+\frac{1}{2}\right)\hbar\omega_{cj}\xi_{nk_y}(x), \tag{5}$$

where $n=0,1,2,\ldots$ is the Landau quantum number, m_j^* is the effective mass of electrons in the jth subband of DQW, $\omega_{cj}=eB/m_j^*$ is the cyclotron frequency in the jth subband, $X_0=-k_yl_H^2$ is the orbital guiding center in the plane, k_y is the electron wave number in the y direction, and $l_H=\sqrt{\hbar/eB}$ is the magnetic length.

The shape of the symmetric DQW potential is chosen as

$$V_{\text{DQW}}(z)=\begin{cases}0 & -d_W-d_B/2<z<-d_B/2\\ & \text{or}\ \ d_B/2<z<d_B/2+d_W\\ V_0 & \text{otherwise},\end{cases}$$

where d_W is the individual QW width, d_B is the middle-barrier width, and V_B is the middle-barrier height. The Hartree potential can be directly calculated from the Poison equation

$$\frac{d}{dz}\left[\epsilon_b(z)\frac{d}{dz}V_H(z)\right]=\frac{e^2}{\epsilon_0}[n(z)-N_{\text{im}}(z)], \tag{6}$$

where ϵ_b is the dielectric constant of bulk material of the QWs and barriers, which varies with z and $n(z)$ is the electron-density function[4]

$$n(z)=\frac{1}{\pi l_H^2}\sum_{n,j}\frac{1}{\exp\left\{\left[E_j+\left(n+\frac{1}{2}\right)\hbar\omega_{cj}-E_f\right]/k_BT\right\}+1}\times|\phi_j(z)|^2, \tag{7}$$

where T is the electron temperature, E_s is the Fermi energy, and $N_{\text{im}}(z)$ is the donor doping density profile,

$$N_{\mathrm{im}}(z) = N_{\mathrm{im}}^{3\mathrm{D}}(z) + \sum_i N_{\mathrm{im}}^{2\mathrm{D}}(i)\,\delta(z - z_1), \tag{8}$$

which includes both selective doping and δ-doping contribution. Here $N_{\mathrm{im}}^{2\mathrm{D}}(i)$ is the sheet density of ith δ-doping layer at $z=z_i$.

The total electron energy including both in-plane and vertical motions is

$$E_{nj} = (n + 1/2)\hbar\omega_{cj} + E_j + V_{nj}^F, \tag{9}$$

where V_{nj}^F is the exchange energy.

From the self-consistent Eqs. (4)–(8), the authors[4] calculated the eigenstate $\Phi_j(z)$ and total eigenenergy E_{nj} in each step and they found an approximately linear increase in the tunneling gap in the lower magnetic fields and the switching of the ground state between the tunneling-split Landau levels—symmetric and antisymmetric—which was explained as a result of the rising screening effect when both lower symmetric and antisymmetric levels are filled. It means that the SAS gap increases along with increasing magnetic field (as it was experimentally shown in Ref. 3) and the SAS gap above the quantum limit should be constant. Therefore, the total splitting Δ_t between the symmetric and antisymmetric energy states of the DQWs consists of two parts: the constant Δ_{SAS} determined by the overlapping of the electron wave functions of DQWs and the changeable tunneling term V_{nj}^F, involving screening factor,

$$\Delta_t = \Delta_{\mathrm{SAS}} + V_{nj}^F. \tag{10}$$

The last term is strongly reduced with the increase in the magnetic field and for B less then that value for which quantum limit begins can be written as

$$V_{nj}^F = -(K_0 - kB), \tag{11}$$

where K_0 is the maximum screening factor in zero magnetic field and $-kB$ is the changeable screening factor increasing with B up to the quantum limit if only the lowest Landau level in the DQW will be filled. Generally, the energy gap Δ_t between symmetric and antisymmetric states in the DQW is proportional to the magnetic field as it was experimentally observed[3]

$$\Delta_t = (\Delta_{\mathrm{SAS}}^s + kB). \tag{12}$$

Parameter Δ_{SAS}^s is the energy gap determined by overlapping of the wave functions and diminished by the screening at zero magnetic field: $\Delta_{\mathrm{SAS}}^s = \Delta_{\mathrm{SAS}} - K_0$.

The model presented above enables us to calculate the LLs energies in the DQWs with rectangular and triangular shapes of QW including its important ingredients—the equations derived by Zawadzki[27] for the LLs energies in rectangular and triangle single QW, which were used earlier.[28] Thus, the basic equations used here are the following:

$$\frac{(E' - E_\perp)(E_g + E' + E_\perp)}{E_g} = E_j, \tag{13}$$

$$E_\perp = -\frac{E_g}{2} - \frac{E_g}{2}\sqrt{1 + \frac{4\mu_B B}{E_g}\left[f_1 \frac{m_0}{m_c^*}\left(n + \frac{1}{2}\right) \pm \frac{1}{2} g_0^* f_2\right]}, \tag{14}$$

$$f_1 = \frac{E_g + \frac{2}{3}\Delta}{E_\perp + E_g + \frac{2}{3}\Delta}$$

$$f_2 = \frac{(E_g + \Delta)\left(E_\perp + E_g + \frac{2}{3}\Delta\right)}{\left(E_g + \frac{2}{3}\Delta\right)(E_\perp + E_g + \Delta)}, \tag{15}$$

where $E' = E \pm (\Delta_{\mathrm{SAS}}^s + kB)$ and E is the unknown nth LLs energy of the jth QW subband which is split into symmetric and antisymmetric states and this splitting is proportional to magnetic field B, $E_\perp$ is the Landau level energy for a bulk semiconductor (we used the notation of Ref. 27), the value of energy of electron state (subband in QW), E_g is the energy gap (between the top of the valence band and the edge of the conduction band), Δ is the spin-orbit splitting, m_0 is the electron mass, m_c^* is the effective electron mass which corresponds to the bottom of the conduction band, g_0^* is effective g factor on the bottom of the conduction band, and μ_B is the Bohr magneton.

Equations (13)–(15) enable us to calculate the electron states in external magnetic fields in the DQW with rectangular shape of QW. If the shape of QWs in the DQW is triangular the next equation substituted Eq. (13), should be used

$$(a+b)a^{1/2}b^{1/2} + (a-b)^2 \ln\left|\frac{b^{1/2} - a^{1/2}}{(b-a)^{1/2}}\right| = \left[\frac{E_g^*}{2m_c^*}\right]^{1/2} 4eF\hbar\pi(j + 3/4), \tag{16}$$

where: $a = E' - E_\perp$; $b = E_g^* + E' + E_\perp$; F is the electric field caused by the interface, which is determined by the potential $U = eFz$.[27]

TABLE I. Parameters of the InGaAs/InAlAs DQW structures.

Sample	Concentration of InAs in the channels (%)	Thickness of the channels (nm)	Thickness of the middle barrier (nm)	The QW profile	Number of δ-doping layers	Donor concentration (according to technologists) 10^{12} cm^{-2}
2506	65	20	20	smooth interface[a]	3	3.5
3181	65	5	5	sharp interface	2	3.5
3183	65	20	20	smooth interface	3	0.5

[a]The smooth interface enables us to obtain a flat edge of the conduction band in the QW (Ref. 28).

C. Role of carriers statistics

In the case of DQWs investigated, the 2DEG density is high and the electron gas is degenerated (it is important for forecasted applications of DQW in the quantum circuits because the resistance of such elements cannot be very large). It means that the MPR theory of the degenerated electron gas[11] should be taken into account to interpret the experimental data. The probability of the electron transition depends on the $f(E)$ distribution function for initial states and on the $[1-f(E')]$ function for finite states. It is approached in the expression for the dissipate current in the x direction, which is proportional to the total number of transitions per second caused by the collisions,

$$J_x \propto \int dE \times \sum_{nn'} \frac{G_{nn'}(E,E+\hbar\omega_{\mathrm{LO}})F(E)[1-F(E+\hbar\omega_{\mathrm{LO}})]}{[E-\hbar\omega_c(n+1/2)]^{1/2}[E+\hbar\omega_{\mathrm{LO}}-\hbar\omega_c(n'+1/2)]^{1/2}}, \tag{17}$$

where $G_{nn'}(E,E')$ is the smoothly varying function of the energies and numbers.

Equation (17) introduces additional resonance condition to the MPR for the degenerated electron gas [despite main condition (3)]. The *electron transitions* with absorption of phonons should cross the Fermi level in order to start from full states and finish on empty states.

It is noticeable from Eq. (7) that the distribution function also plays a significant role in the screening effect. At low temperatures (0.3–4.2 K) the Fermi-Dirac function shape is the precipitous step—the electron states under the Fermi level are occupied and those above the Fermi level are empty. It means that the increase in screening effect noticed by Huang and Manasreh,[4] when both lower symmetric and antisymmetric levels are filled, must be pronounced. At higher temperatures, the distribution function is closer to the Boltzman's functions. Then the LLs release from electrons more slowly along with the increasing magnetic field. This effect (removing of screening) one would expect to be weaker at higher temperatures.

III. EXPERIMENT

A. Description of the structures

The DQWs based on the InGaAs/InAlAs/InP structures were produced by the low-pressure metal organic-vapor phase epitaxy on semi-insulating (100) InP:Fe substrates in the Institute of Electronic Materials Technology, Warsaw. The same production method of the structures with a single QW, which was reported earlier,[28] was also used for production of DQW structures with rectangular, as well as triangular QWs. The structure of the first type (#2506) consists of two $In_{0.65}Ga_{0.35}As$ QW of 20 nm thickness each and three $In_{0.52}Al_{0.48}As$ barriers. In each barrier there, is the donor δ-doping layer as it can be seen in Fig. 1, where the conduction-band-edge profile is shown. The cross section of two types of structures is presented in Fig. 2.

The second DQW structure (#3181) [Fig. 2(b)] consists also of two $In_{0.65}Ga_{0.35}As$ QW (thickness $\tilde{5}$ nm) and three $In_{0.52}Al_{0.48}As$ barriers. However, in this case the barrier between QWs is not doped and the thickness is of 5 nm. The corresponding conduction band shape is shown in Fig. 3. For this particular case, the 2DEG in each QW can be considered as one localized into a triangular potential well (see Fig. 3).

Both of the structures are symmetric with the respect to the middle of central barriers which means that the quantum

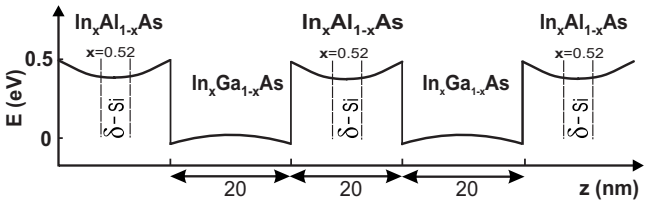

FIG. 1. The conduction-band edge profile of the 2506 structure.

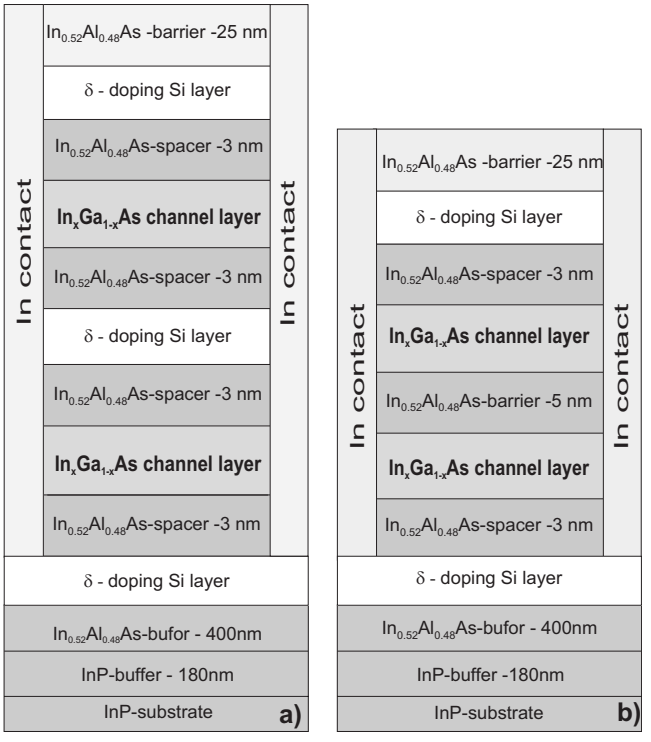

FIG. 2. (a) The cross section of the 2506 structure used in the experiments; (b) the cross section of the 3181 structure.

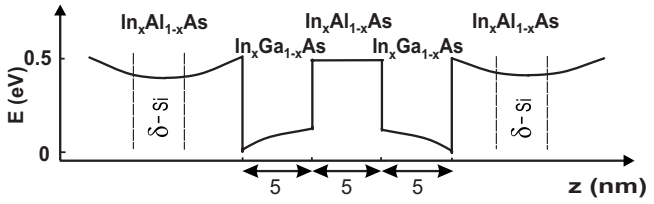

FIG. 3. The conduction-band shape for the sample 3181.

wells are identical and their 2DEG densities are matched with a great probability. The parameters of the structures are listed in Table I. The level of doping is different for structures #2506 and #3183 with rectangular shaped QWs. The pronounced SdH oscillations, as well as integer quantum Hall effect, were clearly seen for all types of structures, namely, for #2506, #3183, and #3181.

The SdH oscillations also undergo the beating effect which was observed earlier[10] for all of these structures. It means that SAS gap without a magnetic field (see Sec. II) was not equal to zero in the DQWs researched.

B. Experiment and results

1. Experimental method

In order to measure the MPR experimentally two methods are used: galvanomagnetic method (measurement of magnetoresistance) and optical method (measurement of photoconductivity in strong magnetic field).[11] In both cases the following fact is used, namely, in high magnetic fields the conductivity σ_{xx} is proportional to the scattering rate and hence, to the joint density of states of the levels separated in energy by the optics phonon energy $\hbar\omega_0$.[19] The conductivity thus exhibits a maximum each time the optic phonon energy is equal to the separation of one or more Landau levels, giving the resonance condition (3). If the criterion of strong magnetic field is fulfilled, the magnetoresistance ρ_{xx} is proportional to σ_{xx} and resistivity shows also a series of maxima. Therefore, usually the magnetoresistance ρ_{xx} is measured to observe MPR.

We have performed the galwanomagnetic measurements in the pulsed magnetic fields generated in the optimal coil buildup,[29] with the capacitor of 10 mF and 3000 V and the energy 45 kJ (duration of pulse 14 ms). The magnetoresistivity $\rho_{xx}(B)$ as a function of magnetic field was registered up to 35 T at different temperatures within the range of 77–200 K. In order to determine the oscillated change in magnetoresistance $\Delta\rho_{xx}(B)$, the background was deducted and the oscillation part of magnetoresistance was separated.

2. Experimental curves

The typical experimental curves of magnetoresistance $\rho_{xx}(B)$ obtained for structure #2506 are shown in Fig. 4. These two curves were registered at temperature 77 K in the pulsed magnetic fields up to 22 T (charging of capacitor to 2 kV) and up to 35 T (charging of capacitor to 3 kV), respectively.

The peaks of magnetoresistance observed against a nonlinear background can clearly be seen here. The amplitude of these peaks increases along with rising magnetic field. It is necessary to substract the monotonic nonlinear background to separate the oscillation part of the magnetoresistance. The final curves of $\Delta\rho_{xx}(B)$ are shown in Fig. 5 where the MPR-oscillations peaks are arranged and the subtle structure of these peaks appears.

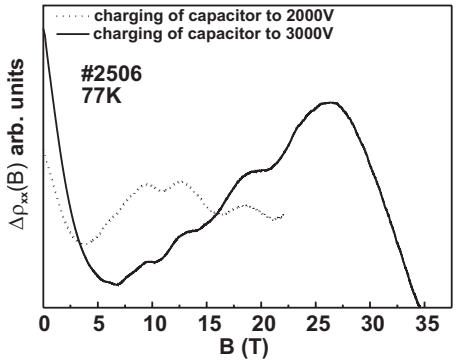

FIG. 4. The transverse magnetoresistance $\rho_{xx}(B)$ for structure 2506 obtained at temperature 77 K with charging of capacitor to 2 kV and to 3 kV.

The experimental curves for the remaining two structures were obtained in this way. In Fig. 6 the $\Delta\rho_{xx}(B)$ curves are presented obtained for the sample #3183, where the MPR oscillations were observed at temperatures from 77 to 125 K (the MPR oscillations are shown for 82 K). The curves of $\Delta\rho_{xx}(B)$ obtained for the structure #3181 are shown in Fig. 7 for $T=86$ K. The curves for this structure differ from previous curves obtained for DQWs with the rectangular shape of QWs because the MPR-oscillation peaks are not pronounced and join together a common band. It is interesting to note that only the oscillation curve for the structure #3183 (Fig. 6) corresponds perfectly to the rule of periodicity in the inverse magnetic field. The increase in temperature above 120 K leads to suppression of MPR oscillations for all three types of structures.

IV. DISCUSSION

To interpret the results obtained on the MPR it is necessary to calculate the LL energies for DQWs investigated.

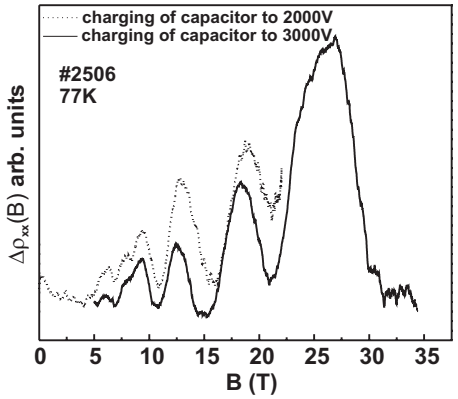

FIG. 5. The oscillation part of magnetoresistance $\Delta\rho_{xx}(B)$ obtained from the curves shown in Fig. 4.

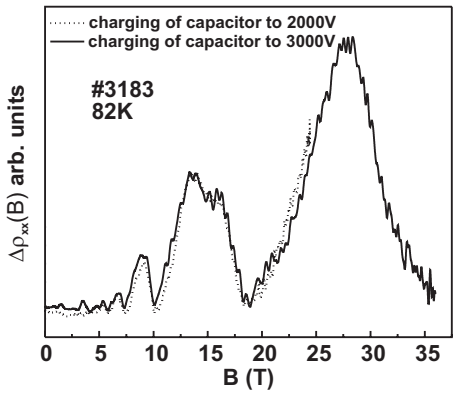

FIG. 6. The MPR oscillations for structure 3183 in the pulse magnetic fields up to 22 T and up to 35 T obtained at 82 K.

Further, we need to know the phonon spectra of these structures regarding both QW and barriers, as was mentioned above.

A. Calculation of the LL energies

Equations (13)–(16) enable us to calculate the electron states in external magnetic fields in DQW for the rectangular or triangular shape of QW, e.g., for the structures #2506 and #3183 as well as #3181. These states can be labeled as $E_{j,a(as),n^{\pm}}$ where j is the quantum number of the QWs subbands, $a(as)$ labeled symmetric or antisymmetric states, and n is number of the LL regarding spin "up" (+) or "down" (–). The equations mentioned above contain a considerable number of parameters, namely, the band structure parameters of QW's material, as well as parameters of QW, and the applied model parameters.

1. Choosing of parameters

In expression (12) for the total splitting of the energy states in the DQWs, the SAS gap have two entries: the first one is constant (Δ_{SAS}) determined by the overlapping of electron wave functions of two QWs and the other which varies with the screening (see Sec. II). If the magnetic field reaches the quantum limit then $\Delta_t = \Delta_{SAS}$ and becomes constant. Obviously, it is important to choose appropriately in Eq. (12) the parameter k is the coefficient of proportionality between the splitting on the symmetric and antisymmetric states and the value of magnetic field B. At low temperatures, this parameter was equal to 0.19 for structures #2506 and #3181,[10] but at higher temperatures the screening becomes less effective as mentioned in Sec. II. This fact is reflected in the value of Δ_{SAS}. This magnitude was determined experimentally at 300 K and was equal to 3.1 meV for the first subband,[30] while at 0.65 K it became equal to 2.0 meV.[10] One can assume that k will be considerably smaller at the temperatures above 77 K. The band-structure parameters for the $In_{0.65}Ga_{0.35}As$ alloy, such as E_g, m^*, Δ, and g^*, are presented in Table II.

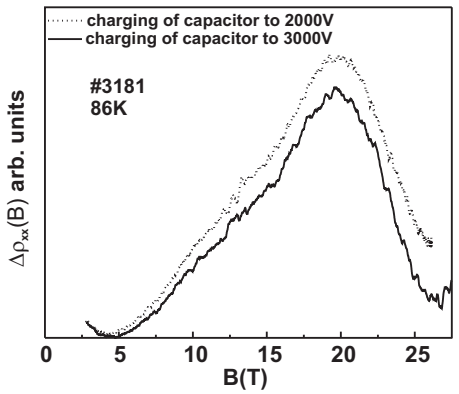

FIG. 7. The MPR curves for structure 3181 in the pulse magnetic fields up to 26 T and up to 30 T obtained at 86 K.

TABLE II. Energy band parameters for the $In_{0.65}Ga_{0.35}As$ QW in the structures 2506, 3181, and 3183 in the region from 77 to 90 K.

x	E_g (eV)	m_c^*/m_0	g_c^*	Δ (eV)
0.65	0.723	0.0229	−9.90	0.355

These parameters for solid solutions can be calculated using their known dependencies on temperature T and composition x taken from the book of Madelung[31] and proved to be correct in the case of single QWs.[28]

2. LLs energies

In Figs. 8 and 9 the calculated Landau levels are shown for the two subbands: symmetric and antisymmetric for structures #2506 and #3183. Both of these structures have the same band shapes of QWs but the 2DEG density is different, which means that the Fermi energy level is also different, namely: 182 meV for #2506 and 108 meV for #3183.[10] In Fig. 10 the $E_{j,a(as),n^{\pm}}(B)$ curves for structure #3181 with triangular shape of QWs are presented.

In our experiments we exceeded the quantum limit and as it is shown below, we observed the transition from the linear SAS-gap dependence on the magnetic field to a constant one after crossing the quantum limit in a high magnetic-field region. This turning point enables us to obtain a satisfactory agreement between theoretical positions of MPR resonances and the peaks observed experimentally.

3. Phonons

The QWs and barriers of the structures researched consist of the solid solutions $In_{0.65}Ga_{0.35}As$ and $In_{0.52}Al_{0.48}As$, respectively. Investigations of the phonons spectra in $In_{0.53}Ga_{0.47}As$ were performed by authors.[32–34]

These results are presented in a review by Nicholas,[19] where also investigations of the MPR in the InGaAs/InAlAs heterostructures obtained in 80th (Refs. 20–23) are discussed too.

It is known[32–34] that the InGaAs solid solutions as well as the InAlAs ones manifest the two-mode behavior. In the case of the $In_{0.53}Ga_{0.47}As$ composition, there are next two LO-phonon frequencies: 233 cm^{-1} InAs-type and 271 cm^{-1}

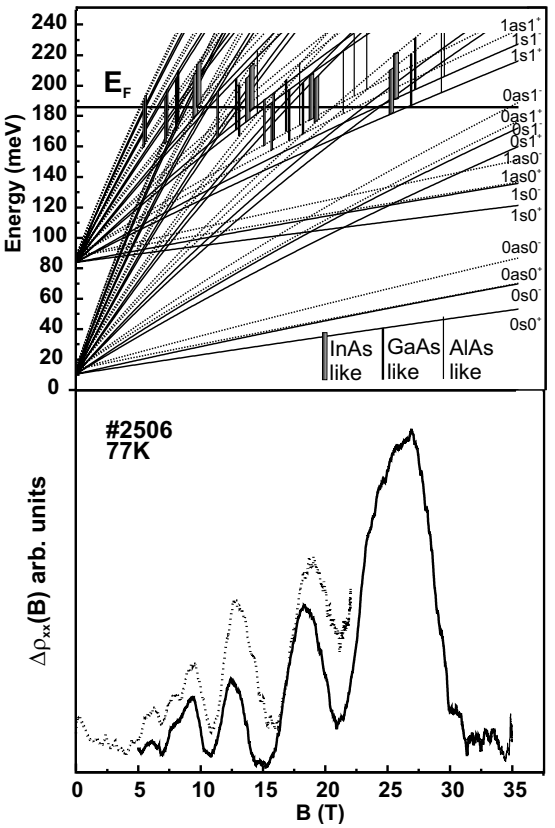

FIG. 8. The MPR oscillation curves and corresponding electron transitions assisted by four kinds of phonons (two kinds of InAs type) for the structure 2506.

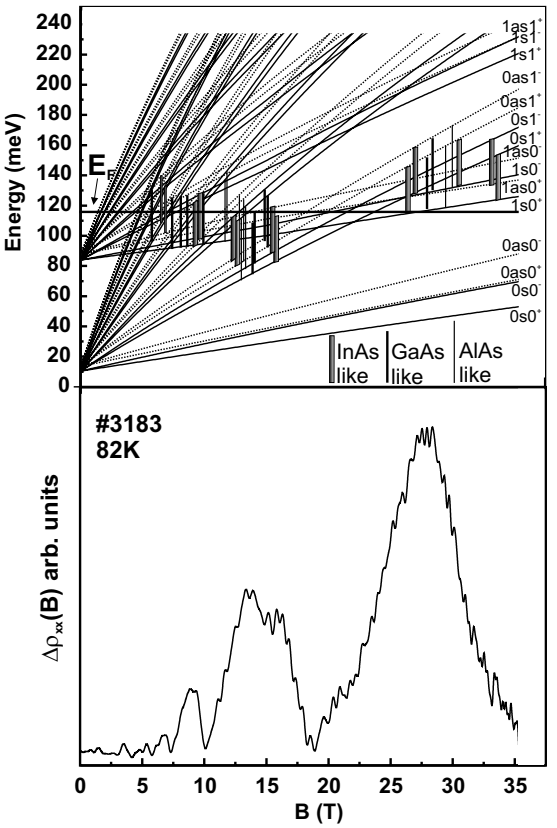

FIG. 9. The MPR oscillation curves and corresponding electron transitions assisted by four kinds of phonons (two kinds of InAs type) for the structure 3183.

GaAs-type.[32] In the MPR researches of the InGaAs/InAlAs heterostructures, two series of the MPR oscillations with phonon's frequencies of 233 and 270 cm^{-1} related to InAs-type and GaAs-type LO phonons, respectively,[20–23] were observed).

In the case of the $In_{0.65}Ga_{0.35}As$ QWs and $In_{0.52}Al_{0.48}As$ barriers, the phonon frequency values of the InAs-type and GaAs-type LO phonons should be little different. Corresponding corrections can be achieved based on the composition dependencies for the InGaAs solid solutions presented in the book of Madelung.[31] In Table III, the data concerning the InAs-type and AlAs-type LO phonons in the $In_{0.65}Ga_{0.35}As$ and $In_{0.52}Al_{0.48}As$ alloys as well as well-known frequencies of the GaAs-type and AlAs-type phonons in the $Al_{0.3}Ga_{0.7}As$ alloy for comparison are presented. It results from Table III that four kinds of the LO phonons should be taken into account at the MPR interpretations in the $In_{0.65}Ga_{0.35}As/In_{0.52}Al_{0.48}As$ DQWs. The energies of these phonons are (i) 28.6 meV (InAs-type LO phonon in QW), (ii) 28.9 meV (InAs-type LO phonon in barrier), (iii) 33.2 meV (GaAs-type LO phonon in QW), and (iv) 40.1 meV (AlAs-type LO phonon in barrier).

Energies (i) and (ii) are too close to be distinguished in the MPR experiment and they probably cause one oscillation series. It is interesting to note that in works (Refs. 32–34) mentioned above, the series of peaks caused by the AlAs-type LO phonons in the InGaAs/InAlAs heterostructures were not observed[32–34] as well as the problem of the interface phonons participation in the MPR was not solved. In works dedicated to MPR in the AlAs/GaAs superlattices[23] and the AlGaAs/GaAs ones,[35] the contribution of the interface or confined phonons in the MPR was not registered. Probably, these phonons do not generate the polarized macropole which electrons could effectively interact with. Hence, these contributions will not be taken into account at the interpretation of the observed MPR oscillations in the DQWs.

4. Interpretation

DQWs with rectangular shaped QW (#2506 and #3183). The electron transitions with the absorption of phonons between the LLs in the DQWs with rectangular shaped of QWs (#2506 and #3183) are shown in Figs. 8 and 9. The fitting parameter $k=0.08$ for the states belonging to the first subband with the Landau number $n=0,\ldots,5$ and equal to 0.06 one for the states belonging to the second subband with the same Landau numbers n. The oscillation curves of MPR are presented there too. It is visible that a group of the electron transitions corresponds to each MPR peak with the absorption of four kinds of the LO phonons presented in Table III. The dominant contribution of the InAs-type LO phonons, both belonging to QW and barriers, is established confidently. They determine the main peaks of the observed MPR oscillations. Some of the shown electron transitions do not cross the Fermi level and it can be seen that their contribution in the resonance peaks is minor.

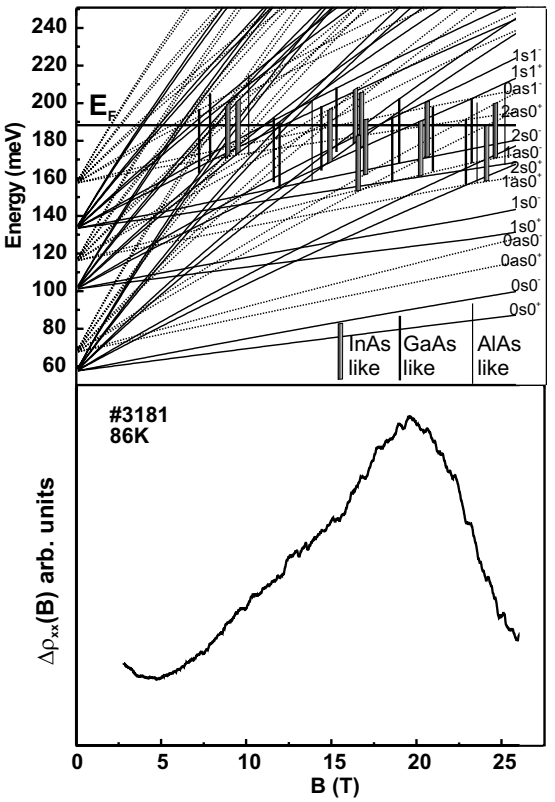

FIG. 10. The MPR oscillation curve and corresponding electron transitions assisted by four kinds of phonons (two kinds of InAs-type LO phonon) for structure 3181.

The quantum limit is not achieved for structure #2506 for both the first and the second sub-bands because the Fermi energy is high (182 meV). In the case of structure #3183, the Fermi level is at 108 meV. The quantum limit is placed at 12 T for the second subband and the slope of the $E_{1,s(as),0^{\pm}}(B)$ functions is changed after the mentioned value of B. The quantum limit for first subband takes place at 23 T and the $E_{0,s(as),0^{\pm}}(B)$ functions as well as the $E_{0,s(as),1^{\pm}}(B)$ one change their slopes. These turns of slopes are important for the interpretation because due to their lack the positions of the $E_{1,s,0^-}-E_{0,as,1^-}$ and $E_{1,s,0^+}-E_{0,as,1^+}$ transitions, which form the main peak at 27 T, would be shifted to low magnetic fields. Then the accordance with the experimental peak would be worse. This possible shift toward higher magnetic fields caused by an exclusion of the screening from the consideration is equal to 2.5 T which is a considerable and experimentally registered value (precision to determine the peak position in our experiment is 0.5%).[36] It is seen in Fig. 9 that the regularity of peak positions, suggesting their periodicity in the inverse magnetic fields for #3183, is apparent and occurs accidentally.

TABLE III. The phonon frequencies and energies in QWs and barriers of researched structures.

L.p	Structure	ν_{LO} (cm^{-1})	E (meV)
1	GaAs-type in $Al_{0.3}Ga_{0.7}As$	271 ± 2	33.60 ± 0.25
2	AlAs-type in $Al_{0.3}Ga_{0.7}As$	333 ± 2	41.29 ± 0.25
3	GaAs-type in $In_{0.65}Ga_{0.35}As$	268 ± 3	33.23 ± 0.37
4	InAs-type in $In_{0.65}Ga_{0.35}As$	231 ± 3	28.64 ± 0.37
5	InAs-type in $In_{0.52}Al_{0.48}As$	233 ± 3	28.89 ± 0.37
6	AlAs-type in $In_{0.52}Al_{0.48}As$	323 ± 3	40.05 ± 0.37

DQW with triangle shape (structure #3181). It was mentioned above that in the case of structure #3181, the resonance curve is different in comparison to the resonance curves for previously investigated structures. We have not the pronounced oscillation peaks in the case of structure #3181 but a wide band consisting of a great number of lines similarly to the optical band in spectroscopy (see Fig. 10). It is caused by a large number of electron transitions with the participation of four kinds of phonons that form this wide band. The electron density in #3181 is the same as in the case of structure #2506 but the shape of QWs is triangular and three subbands are occupied by electrons. The middle barrier in this structure is equal to 5 nm and SAS gap in zero magnetic field, as the optical experiment shows,[30] is equal to 11 meV for first subband and to 17 meV for the second one and 26 meV for the third.

The quantum limit in the third subband is achieved at 5 T and the slope of the $E_{3,s(as),0^{\pm}}(B)$ function changes after this value of B but it is unnoticeable because of the value of the coefficient $k=0.01$. For the second and first subbands, the quantum limit is achieved at magnetic field higher than 35 T.

It is possible to establish that the main maximum at 20 T is formed by the transitions $E_{1,as,0^-}-E_{0,as,1^-}$ and $E_{1,as,0^+}-E_{0,as,1^+}$ with the absorption of InAs-type LO phonons in both QWs and barriers. A swelling of the curve at 10–12 T is caused by participation of the same phonons in the $E_{2,s,0^-}-E_{1,as,1^-}$ and $E_{2,s,0^+}-E_{0,as,3^+}$ transitions. This best fit is reached with coefficient values: $k=0.09$ for first subband and 0.02 and 0.01 for the second and the third, respectively.

V. CONCLUSION

The MPR is investigated in the DQWs of different shapes of QWs and different values of the electron density in the temperature interval from 77 to 90 K in the pulsed magnetic fields up to 37 T. The pronounced MPR oscillations are observed in the case of the DQWs with the quasirectangular shape of QWs and the wide band consisting of a great number of peaks from 5 to 25 T in the case of the triangular shape.

Four kinds of LO phonons are taken into account to interpret the MPR oscillations in the DQW. The peculiarity of the MPR in the DQW is the great number of Landau levels caused by SAS splitting of all electron states. It indicates the contributions of many electron transitions between these levels. This number is multiplied by four kinds of phonons. Therefore, a group of the electron transitions corresponds to each peak. The rule of periodicity of the resonance peaks in inverse magnetic fields does not oblige in this situation. The dominant role of InAs-type LO phonons in forming of MPR peaks in the InGaAs/InAlAs DQW is noticeable.

The kind of carriers statistics is important in the phenomenon of MPR in the DQWs if it contains degenerated 2DEG:

the phonon assistance electron transitions must cross the Fermi level and the screening of exchange interaction is removed by magnetic field. It causes the increase in the SAS gap along with the increase in the magnetic field up to achieving the quantum limit when the antisymmetric state $E_{1,as,0^{\pm}}(B) > E_F$ and the symmetric state $E_{1,s,0^{\pm}}(B) < E_F$. After the quantum limit, the SAS gap becomes constant and this expectation of the Huang and Manasreh[4] model is confirmed.

[1] G. S. Boebinger, H. W. Jiang, L. N. Pfeiffer, and K. W. West, Phys. Rev. Lett. **64**, 1793 (1990).

[2] K. Ensslin, A. Wixforth, M. Sundaram, P. F. Hopkins, J. H. English, and A. C. Gossard Phys. Rev. B **47**, 1366 (1993).

[3] K. M. Brown, N. Turner, J. T. Nicholls, E. H. Linfield, M. Pepper, D. A. Ritchie, and G. A. C. Jones, Phys. Rev. B **50**, 15465 (1994).

[4] Danhong Huang and M. O. Manasreh, Phys. Rev. B **54**, 2044 (1996).

[5] J. P. Eisenstein and A. H. MacDonald, Nature (London) **432**, 691 (2004).

[6] R. M. Lewis, P. D. Ye, L. W. Engel, D. C. Tsui, L. N. Pfeiffer, and K. W. West, Phys. Rev. Lett. **89**, 136804 (2002).

[7] R. M Lewis, Yong P. Chen, L. W. Engel, D. C. Tsui, L. N. Pfeiffer, and K. W. West, Phys. Rev. B **71**, 081301(R) (2005).

[8] G. Gervais, H. L. Stormer, D. C. Tsui, L. W. Engel, P. L. Kuhns, W. G. Moulton, A. P. Reyes, L. N. Pfeiffer, K. W. Baldwin, and K. W. West, Phys. Rev. B **72**, 041310(R) (2005).

[9] L. A. Tracy, J. P. Eisenstein, L. N. Pfeiffer, and K. W. West, Phys. Rev. B **73**, 121306(R) (2006).

[10] M. Marchewka, E. M. Sheregii, I. Tralle, D. Ploch, G. Tomaka, M. Furdak, A. Kolek, A. Stadler, K. Mleczko, D. Zak, W. Strupinski, A. Jasik, and R. Jakiela, Physica E (Amsterdam) **40**, 894 (2008).

[11] Y. A. Firsov, V. L. Gurevich, R. V. Parfeniev, and I. M. Tsidlikovskii, in *Landau Level Spectroscopy*, Modern Problems in Condensed Matter Sciences Vol. 27.2, edited by V. M. Agranovich and A. A. Maradudin (North-Holland, Amsterdam, 1991), pp. 1181–1302.

[12] S. F. Fischer, G. Apetrii, U. Kunze, D. Schuh, and G. Abstreiter, Nat. Phys. **2**, 91 (2006).

[13] B. V. Robouch, A. Kisiel, and E. M. Sheregii, Phys. Rev. B **64**, 073204 (2001).

[14] J. Cebulski, E. M. Sheregii, J. Polit, A. Marcelli, M. Piccinini, A. Kisiel, I. Kucherenko, and R. Triboulet, Appl. Phys. Lett. **92**, 121904 (2008).

[15] E. M. Sheregii, Yu. O. Ugrin, D. D. Shuptar, and O. M. Leshko, JETP Lett. **47**, 711 (1988).

[16] E. M. Sheregii and Yu. Ugrin, Sov. Phys. Solid State **32**, 27 (1990).

[17] J. Cebulski, W. Gebicki, V. I. Ivanov-Omskii, J. Polit, and E. M. Sheregii, J. Phys.: Condens. Matter **10**, 8587 (1998); E. M. Sheregii, J. Cebulski, J. Polit, V. I. Ivanov-Omskii, and W. Gêbicki, Semiconductors **32**, 901 (1998).

[18] J. Cebulski, T. Kakol, J. Polit, E. M. Sheregii, D. Poch, I. M. Gorbatiuk, and I. M. Rarenko, J. Alloys Compd. **371**, 103 (2004).

[19] R. J. Nicholas, in *Landau Level Spectroscopy*, Modern Problems in Condensed Matter Sciences Vol. 27.2, edited by V. M. Agranovich and A. A. Maradudin (North-Holland, Amsterdam, 1991), pp. 777–816.

[20] D. Gauthier, L. Dmowski, J. C. Portal, D. Leadley, M. A. Hopkins, M. A. Brummell, R. J. Nicholas, M. Razeghi, and P. Maurel, Superlattices Microstruct. **4**, 201 (1988).

[21] J. C. Portal, G. Gregoris, M. A. Brummell, M. Razeghi, M. A. Di Forte-Poisson, K. Y. Cheng, and A. Y. Cho, Surf. Sci. **142**, 368 (1984).

[22] J. C. Portal, J. Cisowski, R. J. Nicholas, M. A. Brummell, M. Razeghi, and M. A. Poisson, J. Phys. C **16**, L573 (1983).

[23] M. A. Brummell, R. J. Nicholas, J. C. Portal, M. Razeghi, and M. A. Poisson, Physica B & C **117–118**, 753 (1983).

[24] P. Gassot, J. Genoe, D. K. Maude, J. C. Portal, K. S. H. Dalton, D. M. Symons, R. J. Nicholas, F. Aristone, J. F. Palmier, and F. Laruelle, Phys. Rev. B **54**, 14540 (1996).

[25] G. Tomaka, J. Cebulski, E. M. Sheregii, W. Sciuk, W. Strupiriski, and L. Dobrzanski, Acta Phys. Pol. A **94**, 597 (1998).

[26] H. Fröhlich, Adv. Phys. **3**, 325 (1954).

[27] W. Zawadzki, J. Phys. C **16**, 229 (1983).

[28] G. Tomaka, E. M. Sheregii, T. Kakol, W. Strupinski, R. Jakiela, A. Kolek, A. Stadler, and K. Mleczko, Cryst. Res. Technol. **38**, 407 (2003); E. M. Sheregii, D. Ploch, M. Marchewka, G. Tomaka, A. Kolek, A. Stadler, K. Mleczko, W. Strupiński, A. Jasik, and R. Jakiela, Low Temp. Phys. **30**, 858 (2004).

[29] T. Kakol and E. M. Sheregii, Physica B **298**, 594 (2001).

[30] M. Marchewka, E. M. Sheregii, A. Marcelli, M. Piccinini, and J. Cebulski (unpublished).

[31] O. Madelung, *Semiconductor: Basic Data*, 2nd ed. (Springer-Verlag, Berlin, 1996).

[32] M. Brodsky and G. Lucovsky, Phys. Rev. Lett. **21**, 990 (1968).

[33] T. P. Pearsall, R. Carles, and J. C. Portal, Appl. Phys. Lett. **42**, 436 (1983).

[34] A. Pinczuk, J. M. Worlock, R. E. Nahory, and M. A. Pollack, Appl. Phys. Lett. **40**, 826 (1978).

[35] H. Noguchi, H. Sakaki, T. Takamasu, and N. Miura, Phys. Rev. B **45**, 12148 (1992).

[36] Obviously, the 3% uncertainty takes place in the determination of the resonance positions at the pulse magnetic field, but we calibrate the measurements system by the well-known MPR peaks in *n*-InSb what enable us to decrease this uncertainty to 0.5%.